Journal of Solid State Chemistry **151,** 170–180 (2000)
doi:10.1006/jssc.1999.8631, available online at http://www.idealibrary.com on IDEAL®

Crystal Structure of $Ca_{4.78}Cu_6O_{11.60}$

Ph. Galez,[1] M. Lomello-Tafin, Th. Hopfinger, Ch. Opagiste, and Ch. Bertrand

LAIMAN—Université de Savoie, 9 Rue de l'Arc-en-Ciel, BP 240, F-74942 Annecy-le-Vieux Cedex, France

Received October 12, 1999; in revised form January 4, 2000; accepted January 20, 20000

The crystal structure of $Ca_{4.78}Cu_6O_{11.60}$ (crystal system, monoclinic; space group $P2/c$, $Z = 4$, $\rho = 4.48(2)$ g/cm^3, $a = 10.9456(4)$ Å, $b = 6.3192(2)$ Å, $c = 16.8408(5)$ Å, and $\beta = 104.952(2)^\circ$) has been solved and refined using X-ray and neutron powder diffraction combined with Rietveld analysis. It is closely related to the $NaCuO_2$-type structure. The phase stoichiometry and the displacements of atoms with respect to their positions in the previously reported substructure (crystal system, orthorhombic; space group, $Fmmm$, $a = 2.807(1)$ Å, $b = 6.351(2)$ Å, and $c = 10.597(3)$ Å) are explained by the minimization of Ca–Ca repulsion and by a relaxation toward a more regular octahedral environment for Ca atoms. The substitution of Tl atoms for Ca atoms results in an increased thermal stability and in incommensurate structures with modulation vectors depending strongly on the Tl content. © 2000 Academic Press

Key Words: **$Ca_{4.78}Cu_6O_{11.60}$; crystal structure; substitution effects.**

1. INTRODUCTION

In the course of a study on phase equilibria in the Tl–Ba–Ca–Cu–O system and especially along the Tl-1223–Tl-2223 line (1), we found that an oxide containing Ca, Tl, and Cu atoms played an important role, preventing, under our experimental conditions, the formation of the Tl-2223 phase when the Tl content exceeds ~ 1.7–1.8 atoms per formula unit. X-ray diffraction analysis revealed that this phase was closely related to $Ca_5Cu_6O_{12}$ (2–4) and SEM EDX measurements showed that Ca atoms were partly substituted by Tl atoms leading to the hypothetical formula $(Ca, Tl)_5Cu_6O_{12}$. A phase with similar composition, $(Ca_{1-x}Tl_x)_4Cu_5O_{9+y}$, $x = 0.12$–0.20, had already been reported by Dong *et al.* (5). Several ceramic samples with nominal compositions $Ca_5Cu_6O_z$ and $(Ca_{0.73}Tl_x)CuO_z$, $x = 0.2$ and $x = 0.4$, were prepared and it turned out that none of the resulting X-ray diffraction patterns could be satisfactorily explained on the basis of the available structural data (3, 4). We therefore undertook a study of the crystal structure of $Ca_5Cu_6O_{12}$ and its evolution when Tl is partly substituted for Ca.

$Ca_5Cu_6O_{12}$ was first reported for composition $CaCuO_2$ by Roth *et al.* (2). It is formed by the peritectoid reaction $5Ca_2CuO_3 + 7CuO + O_2 \rightarrow 2Ca_5Cu_6O_{12}$ around 800°C and is stable down to room temperature. Using X-ray powder diffraction, the authors proposed an orthorhombic subcell, space group $Cmca$, $a = 10.588(1)$ Å, $b = 2.8122(4)$ Å, and $c = 6.3245(6)$ Å. Weak superstructure reflections seen on precession photographs indicated a monoclinic supercell with space group $C2/c$ or equivalent, $a = 10.946$ Å, $b = 6.345$ Å, $c = 33.72$ Å, and $\beta = 105.5^\circ$. Using X-ray single-crystal diffraction, Siegrist *et al.* (3) confirmed that the subcell was orthorhombic. A refinement based on substructure reflections and carried out in space group $Fmmm$ ($a = 2.807(1)$ Å, $b = 6.351(2)$ Å, and $c = 10.597(3)$ Å) showed that the average structure was closely related to the $NaCuO_2$-type structure (6). It contains linear chains of edge-shared CuO_4 squares directed along [100] with Ca atoms located in half of the octahedral sites in the channels produced by the chains (Fig. 1). These authors also found different supercells with a 5-, 10-, or 12-fold a axis. For the former, a refinement was carried out in space group $Pnca$ (standard setting $Pbcn$, $a = 6.351(2)$ Å, $b = 10.597(3)$ Å, and $c = 14.035(3)$ Å), yielding a stoichiometry of $Ca_4Cu_5O_{10}$ consistent with a ratio of the Cu–Cu to the Ca–Ca distance of 4:5 that is a Ca–Ca spacing of roughly 3.46 Å. Babu and Greaves (4) confirmed, from neutron powder diffraction data, that the substructure was satisfactorily described in space group $Fmmm$ and proposed the stoichiometry $Ca_6Cu_7O_{14}$. Extensive electron diffraction and microscopy work by Milat *et al.* (7–9) revealed that the supercell was actually monoclinic with $a \approx 16.80$ Å, $b \approx 6.32$ Å, $c \approx 10.95$ Å, and $\beta \approx 75^\circ$. Different models of atom arrangement were proposed in which, on average, there are five Ca atoms for six Cu atoms along a resulting in a stoichiometry of $Ca_5Cu_6O_{12}$ (or $Ca_{0.83}CuO_2$). Electron diffraction patterns indicated that both commensurate or incommensurate superstructures could occur. It is worth pointing out that the supercell proposed by Milat *et al.* (7–9) is closely related

[1]To whom correspondence should be addressed. Fax: (33) 4 50 09 23 79 or (33) 4 50 27 65 35. E-mail: philippe.galez@univ-savoie.fr.

0022-4596/00 $35.00

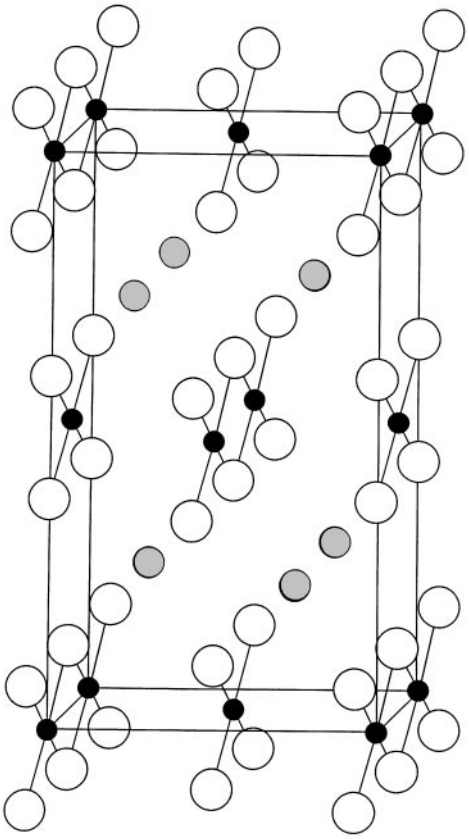

FIG. 1. Orthorhombic subcell of $Ca_5Cu_6O_{12}$. Open, shaded, and dark circles denote O, Ca, and Cu atoms, respectively.

to that reported by Roth *et al.* (2), the only difference, after applying the appropriate transformation, being a translation vector of 16.80 Å instead of 33.72 Å.

It has also been shown that Ca atoms could be partially replaced by Na, Y, Nd, and Gd atoms, the solid solution $(Ca_{1-x}M_x)_{1-y}CuO_2$ extending to $x = 0.15$, $x = 0.50$, $x = 0.67$, and $x = 0.56$, respectively (10–13). In this case, the superstructure is a very sensitive function of the Ca:*M* ratio and of the size of *M*. In general it is incommensurate along and perpendicular to the chains yielding uncertain stoichiometries.

$(Ca_{1-x}M_x)_{1-y}CuO_2$ phases are suitable for studying the magnetic properties of linear chains of edge-shared CuO_4 squares (14–18) which are also found in $(Sr_8Ca_6)Cu_{24}O_{41}$ (19) and $(Ca_8La_6)Cu_{24}O_{41}$ (20) together with ladders. This constituted an extra motivation for the present work.

We report here on an X-ray and neutron powder diffraction study on $Ca_5Cu_6O_{12}$ and $(Ca_{1-x}Tl_x)_{1-y}CuO_2$. The structure of the unsubstituted phase is solved starting from a model of atom arrangement built with information given in Refs. (2, 3, 7–9). The effect of Tl substitution is compared with that of rare-earth atom substitution.

2. EXPERIMENTAL

2.1. Sample Preparation

The Tl-free samples, hereafter labeled S1 and S2, were prepared by solid-state reaction from $CaCO_3$(99.95%) and CuO (99.99%) with a Ca:Cu ratio of 0.83:1. The mixtures were heated for six (S1) or five (S2) periods of 17 h in flowing oxygen (room pressure) at 790°C with 10°C/min heating and cooling rates. The samples were ground and pelletized prior to each treatment. The final powders were found to contain small amounts of CaO, Ca_2CuO_3, and CuO, indicating that equilibrium had not been reached despite long annealing time. The reaction rate appears to be significantly lower than it is when precipitation routes are used (2, 3). However, the presence of impurity phases does not affect the stoichiometry of the title compound since XRD analysis of other samples with Ca:Cu ratios between 0.6:1 and 1.1:1 and prepared exactly in the same way showed that there is no solid solubility: no changes of the cell parameters could be detected. The presence of Ca_2CuO_3 also indicates that the sintering temperature, 790°C, is higher than the temperature of the invariant $6Ca_2CuO_3 + 1/2O_2 \rightarrow 7CaO + Ca_5Cu_6O_{12}$.

$(Ca_{0.73}Tl_x)CuO_2$ samples with $x = 0.2$ (S3) and $x = 0.4$ (S4) were sintered in sealed quartz tubes at 890°C, $p(O_2) = 2$ bar for 12 h. The starting mixtures with CuO, Tl_2O_3 (99.5%), and prefired CaO (99%) were pressed into pellets and wrapped in gold foils before sealing. Unfortunately, the Tl content in the reacted ceramics could not be estimated from weight losses because of a reaction at the interface between the pellets and the gold foils. Both Tl-free and Tl-containing powders are black.

2.2. X-Ray and Neutron Diffraction

All samples were characterized by X-ray diffraction using a powder diffractometer (Co$K\alpha$) equipped with the position-sensitive detector INEL-CPS 120. Additional X-ray data were collected for the refinement of the structure of $Ca_5Cu_6O_{12}$ in S1 on a Philips PW1050 powder goniometer with Bragg–Brentano geometry (Cu $K\alpha$, graphite monochromator, room temperature, $4° \leq 2\theta \leq 90°$, 0.03° 2θ step, 18 s step time). Neutron data were collected from S2 on the high-resolution powder diffractometer D2B at the Institut Laue Langevin in Grenoble ($\lambda = 1.5944$ Å, Ge (335) monochromator, room temperature, $0° < 2\theta \leq 162.5°$, 0.05° 2θ step, 250 s step time). The crystal structures were refined using the program Fullprof (21). As already mentioned, S1 and S2 were found to contain small amounts of Ca_2CuO_3, CaO, and CuO. These phases were included in the refinements. Details about the refinement procedure are given in Section 4.1.

3. STRUCTURE MODELS FOR $Ca_5Cu_6O_{12}$

As mentioned in the Introduction, both X-ray precession photographs (2) and electron diffraction (7–9) indicated a monoclinic supercell with $a \approx 10.95$ Å, $b \approx 6.32$ Å, $c \approx 33.72$ or 16.84 Å, and $\beta \approx 105.5°$. Indeed our powder diffraction patterns could be completely indexed on the basis of the cell with the short **c** translation vector (16.84 Å) which yields a six-fold superstructure along the chains. This supercell was therefore adopted. It is derived from the *Fmmm* subcell (3) by applying the transformation $\mathbf{a}_m = \mathbf{c}_0 - \mathbf{a}_0$, $\mathbf{b}_m = -\mathbf{b}_0$, and $\mathbf{c}_m = 6\mathbf{a}_0$. Another important piece of information was given by Siegrist *et al.* (3) who observed, on a difference Patterson map, a strong peak corresponding to a distance of 3.46 Å and assigned it to the mean Ca–Ca spacing. This means that Ca atoms are more or less regularly distributed along the channels and that there are five Ca atom sites for six Cu atom sites since $3.46 \times 5 = 17.3 \approx 16.84$, yielding a stoichiometry of $Ca_5Cu_6O_{12}$ as suggested by Milat *et al.* (7–9). Taking this information into account, two models of atom arrangement were built (Fig. 2). The coordinates of the Cu and O atoms with respect to an

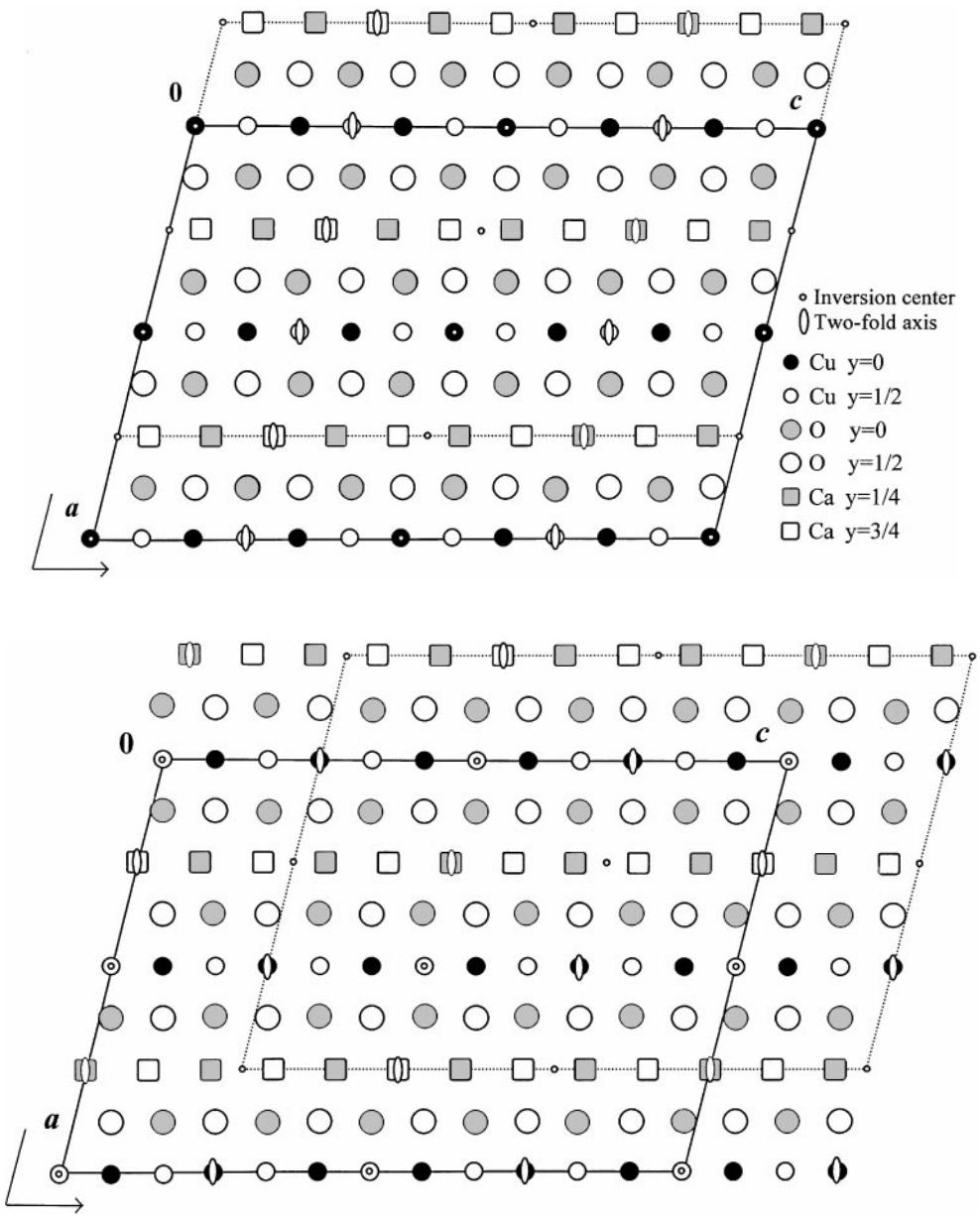

FIG. 2. Models of atom arrangement for $Ca_5Cu_6O_{12}$. (a) Model 1 and (b) model 2.

TABLE 1
Sets of Calculated Atom Coordiantes for Models 1 and 2 with Different Origin Choices (See Text)

	Set 1a				Set 1b				Set 2a				Set 2b			
Atom	WP	x	y	z	WP	x	y	z	WP	x	y	z	WP	x	y	z
Cu	2*a*	0	0	0	4*g*	0.250	0.000	0.000	4*g*	0.000	0.000	0.083	4*g*	0.250	0.000	0.000
	4*g*	0.000	0.000	0.167	4*g*	0.250	0.000	0.167	2*e*	0	0.000	$\frac{1}{4}$	4*g*	0.250	0.000	0.167
	4*g*	0.000	0.500	0.083	4*g*	0.250	0.000	0.333	4*g*	0.500	0.000	0.083	4*g*	0.250	0.000	0.333
	2*e*	0	0.500	$\frac{1}{4}$	4*g*	0.250	0.500	0.083	2*f*	$\frac{1}{2}$	0.000	$\frac{1}{4}$	4*g*	0.250	0.500	0.083
	2*d*	$\frac{1}{2}$	0	0	4*g*	0.250	0.500	0.250	2*c*	0	$\frac{1}{2}$	0	4*g*	0.250	0.500	0.250
	4*g*	0.500	0.000	0.167	4*g*	0.250	0.500	0.416	4*g*	0.000	0.500	0.167	4*g*	0.250	0.500	0.416
	4*g*	0.500	0.500	0.083					2*b*	$\frac{1}{2}$	$\frac{1}{2}$	0				
	2*f*	$\frac{1}{2}$	0.500	$\frac{1}{4}$					4*g*	0.500	0.500	0.167				
Ca	4*g*	0.250	0.750	0.450	4*g*	0.000	0.250	0.150	4*g*	0.250	0.250	0.100	4*g*	0.000	0.250	0.150
	4*g*	0.250	0.750	0.050	4*g*	0.000	0.250	0.550	4*g*	0.250	0.250	0.300	4*g*	0.000	0.250	0.550
	4*g*	0.250	0.750	0.850	2*e*	0	0.250	$\frac{3}{4}$	4*g*	0.250	0.250	0.500	2*e*	0	0.250	$\frac{3}{4}$
	4*g*	0.250	0.750	0.650	4*g*	0.500	0.250	0.150	4*g*	0.250	0.250	0.700	4*g*	0.500	0.250	0.050
	4*g*	0.250	0.750	0.250	4*g*	0.500	0.250	0.550	4*g*	0.250	0.250	0.900	2*f*	$\frac{1}{2}$	0.250	$\frac{1}{4}$
					2*f*	$\frac{1}{2}$	0.250	$\frac{3}{4}$					4*g*	0.500	0.250	0.65
O	4*g*	0.378	0.000	0.396	4*g*	0.128	0.000	0.063	4*g*	0.122	0.000	0.020	4*g*	0.128	0.000	0.063
	4*g*	0.378	0.000	0.063	4*g*	0.128	0.000	0.230	4*g*	0.122	0.000	0.187	4*g*	0.128	0.000	0.230
	4*g*	0.378	0.000	0.230	4*g*	0.128	0.000	0.396	4*g*	0.122	0.000	0.354	4*g*	0.128	0.000	0.396
	4*g*	0.122	0.000	0.104	4*g*	0.372	0.000	0.104	4*g*	0.122	0.500	0.104	4*g*	0.128	0.500	0.146
	4*g*	0.122	0.000	0.437	4*g*	0.372	0.000	0.270	4*g*	0.122	0.500	0.270	4*g*	0.128	0.500	0.313
	4*g*	0.122	0.000	0.270	4*g*	0.372	0.000	0.437	4*g*	0.122	0.500	0.437	4*g*	0.128	0.500	0.480
	4*g*	0.122	0.500	0.020	4*g*	0.128	0.500	0.146	4*g*	0.378	0.000	0.146	4*g*	0.372	0.000	0.104
	4*g*	0.122	0.500	0.354	4*g*	0.128	0.500	0.313	4*g*	0.378	0.000	0.313	4*g*	0.372	0.000	0.270
	4*g*	0.122	0.500	0.187	4*g*	0.128	0.500	0.480	4*g*	0.378	0.000	0.480	4*g*	0.372	0.000	0.437
	4*g*	0.378	0.500	0.480	4*g*	0.372	0.500	0.020	4*g*	0.378	0.500	0.063	4*g*	0.372	0.500	0.020
	4*g*	0.378	0.500	0.146	4*g*	0.372	0.500	0.187	4*g*	0.378	0.500	0.230	4*g*	0.372	0.500	0.187
	4*g*	0.378	0.500	0.313	4*g*	0.372	0.500	0.354	4*g*	0.378	0.500	0.396	4*g*	0.372	0.500	0.354

arbitrary origin were first derived from the corresponding positions in the subcell. The two "zig-zag" sets of regularly distributed Ca atoms were then placed in the channels in such a way that symmetry elements appeared at z, $z + \frac{1}{4}$, $z + \frac{1}{2}$, and $z + \frac{3}{4}$. The only difference between the two models comes from a relative shift along [001] between the two sets of Ca atoms. In model 1 (Fig. 2a), the y coordinates of Ca atoms alternate along **c** and $\mathbf{c} \times \mathbf{b}$ whereas, in model 2 (Fig. 2b), they alternate only along **c**. In both cases, symmetry elements are two-fold axes, inversion centers, and glide planes *c*, which is consistent with space groups $P2/c$, Pc, and $P2$. We first concentrated on space group $P2/c$ which finally gave satisfactory results as will be seen in the next sections. For each model, two origin choices are possible depending on the remaining symmetry elements in the real structure. This resulted in four sets of atom coordinates given in Table 1 and labeled 1a, 1b, 2a, and 2b:

—1a = model 1 with cell indicated by plain lines in Fig. 2a,

—1b = model 1 with cell indicated by dotted lines in Fig. 2a,

—2a = model 2 with cell indicated by plain lines in Fig. 2b,

—2b = model 2 with cell indicated by dotted lines in Fig. 2b.

X-ray powder diffraction patterns were simulated for both models (Fig. 3). Here the origin choice is not relevant since the atoms are in "ideal" positions. It is readily seen from Fig. 3 that the first model yields a diffraction pattern in good agreement with the experimental one. For model 2 however, the main superstructure reflections do not appear at the correct Bragg angle. Structure refinements using X-ray and neutron data from S1 and S2, respectively, were then performed starting from sets of coordinates 1a and 1b. It soon appeared that the best results were obtained using set 1a, which was finally retained.

4. RESULTS

4.1. Rietveld Analysis of Tl-Free Samples

(*a*) *X-rays.* Because of the large number of parameters to be varied, the refinement was conducted stepwise. In the

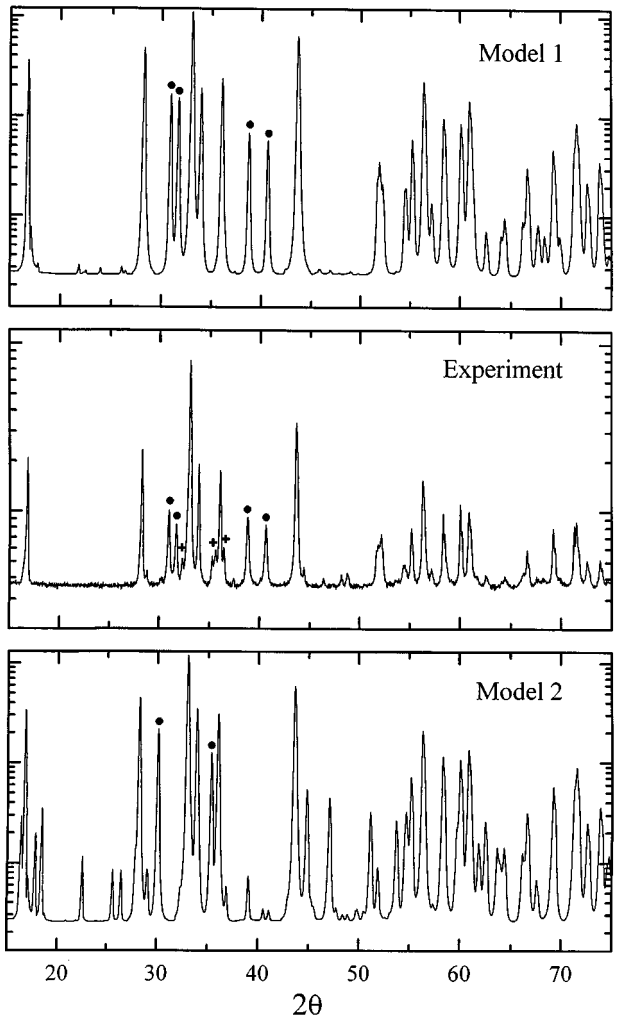

FIG. 3. Simulated X-ray diffraction pattern for model 1 (top) and model 2 (bottom). X-ray diffraction pattern of S1 (middle). The closed circles denote the main superstructure reflections from $Ca_5Cu_6O_{12}$ and the crosses the reflections arising from impurity phases. Cu$K\alpha$; 2θ angular range, 10–90°; logarithmic representation.

first stage, the scale factor, the cell parameters, the atom coordinates, the isotropic displacement parameters, the profile shape parameters, and the asymmetry, texture, and mixing coefficients for each phase were varied successively. Then, only the scale factor and the cell parameters allowed to vary for the impurity phases. No attempt was made to refine the occupancy parameters and all sites for all phases were considered fully occupied. In the final stage of the refinement, 59 parameters were varied freely including the coordinates for Cu and Ca atoms in $Ca_5Cu_6O_{12}$ and three isotropic displacement parameters, one for each chemically different ion. The background was computed with the usual polynomial function and the Pearson VII profile function was used for peak fitting. The refinement was based on diffraction data in the range $14° \leq 2\theta \leq 90°$, containing 911 reflections from the main $Ca_5Cu_6O_{12}$ phase, 48 from Ca_2CuO_3, 7 from CaO, and 35 from CuO. Final profile and Bragg agreement factors are given in Table 2 together with the weight fraction and the cell parameters for each phase. The final refined positional and isotropic displacement parameters for $Ca_5Cu_6O_{12}$ are given in Table 3. Note that the standard uncertainties for O atom coordinates are not given because these coordinates were not refined during the last cycles.

(*b*) *Neutrons.* Structure refinement from neutron data (S2) was carried out in the same way except that O atom

TABLE 2
Weight Fraction and Cell Parameters of the Individual Phases in S1 and S2

	S1, Cu$K\alpha$	S2, Neutrons 1.5944 Å, D2B, ILL
R_p (%)	2.45	4.18
R_{wp} (%)	3.37	5.49
S	2.31	2.03
$Ca_5Cu_6O_{12}$, $P2/c$, $Z = 4$		$Ca_{4.78}Cu_6O_{11.60}$
Weight fraction (%)	92.4(7)	89.8(7)
a (Å)	10.9459(6)	10.9456(4)
b (Å)	6.3197(4)	6.3192(2)
c (Å)	16.839(1)	16.8408(5)
β (°)	104.943(4)	104.952(2)
V (Å^3)	1125.4(1)	1125.39(6)
R_{Bragg} (%)	4.70	3.28(5.75)[a]
Number of reflections	911	2211 (1540)[b]
Ca_2CuO_3, $Immm$, $Z = 2$		
Weight fraction (%)	3.57(11)	3.75(8)
a (Å)	12.238(5)	12.236(3)
b (Å)	3.776(2)	3.7779(6)
c (Å)	3.258(1)	3.2590(6)
V (Å^3)	150.6(1)	150.65(5)
R_{Bragg} (%)	8.60	5.00
Number of reflections	48	103
CaO, $Fm\bar{3}m$, $Z = 4$		
Weight fraction (%)	0.29(14)	0.83(3)
a (Å)	4.80(1)	4.809(1)
V (Å^3)	110.6(5)	111.24(5)
R_{Bragg} (%)	15.1	3.01
Number of reflections	7	15
CuO, $C2/c$, $Z = 4$		
Weight fraction (%)	3.74(11)	5.67(11)
a (Å)	4.687(4)	4.689(1)
b (Å)	3.419(3)	3.4185(6)
c (Å)	5.128(5)	5.133(1)
β (°)	99.60(5)	99.42(2)
V (Å^3)	81.0(1)	81.17(3)
R_{Bragg} (%)	3.34	4.92
Number of reflections	35	81

[a] R_{Bragg} on observed superstructure reflections.
[b] Number of observed superstructure reflections.

TABLE 3
Fractional Atom Coordinates, Isotropic Displacement Parameters (Å^2), and Site Occupancies in the Structure of $Ca_5Cu_6O_{12}$

		S1, Cu$K\alpha$				S2, Neutrons, 1.5944 Å				
Atom	WP	x	y	z	B (Å^2)	x	y	z	B (Å^2)	Occ.
Cu1	2*a*	0	0	0	0.86(4)	0	0	0	0.52(3)	
Cu2	4*g*	0.0063(18)	0.0074(20)	0.1712(9)	0.86(4)	− 0.0031(13)	0.0073(16)	0.1698(6)	0.52(3)	
Cu3	4*g*	− 0.0051(18)	0.511(4)	0.0806(9)	0.86(4)	− 0.0052(11)	0.5155(15)	0.0770(6)	0.52(3)	
Cu4	2*e*	0	0.515(5)	$\frac{1}{4}$	0.86(4)	0	0.5178(22)	$\frac{1}{4}$	0.52(3)	
Cu5	2*d*	$\frac{1}{2}$	0	0	0.86(4)	$\frac{1}{2}$	0	0	0.52(3)	
Cu6	4*g*	0.5057(19)	0.0115(19)	0.1679(10)	0.86(4)	0.4997(12)	0.0158(16)	0.1660(6)	0.52(3)	
Cu7	4*g*	0.4927(18)	0.507(3)	0.0796(9)	0.86(4)	0.4968(13)	0.5047(21)	0.0807(8)	0.52(3)	
Cu8	2*f*	$\frac{1}{2}$	0.515(4)	$\frac{1}{4}$	0.86(4)	$\frac{1}{2}$	0.508(3)	$\frac{1}{4}$	0.52(3)	
Ca1	4*g*	0.2426(20)	0.760(4)	0.4612(12)	0.73(10)	0.2447(18)	0.745(3)	0.4515(10)	0.43(6)	
Ca2	4*g*	0.2534(22)	0.748(5)	0.0653(11)	0.73(10)	0.2467(18)	0.743(3)	0.0479(10)	0.43(6)	
Ca3	4*g*	0.2588(21)	0.741(4)	0.8588(11)	0.73(10)	0.2593(22)	0.745(4)	0.8565(11)	0.43(6)	0.78(3)
Ca4	4*g*	0.2556(24)	0.746(4)	0.6383(12)	0.73(10)	0.2513(18)	0.748(3)	0.6555(9)	0.43(6)	
Ca5	4*g*	0.2412(24)	0.748(3)	0.2492(12)	0.73(10)	0.2593(16)	0.751(3)	0.2680(8)	0.43(6)	
O1	4*g*	0.287	− 0.162	0.361	0.62(8)	0.3743(13)	− 0.0767(20)	0.3906(9)	0.58(3)	
O2	4*g*	0.382	0.060	0.064	0.62(8)	0.3768(16)	0.0664(25)	0.0689(9)	0.58(3)	
O3	4*g*	0.383	0.079	0.238	0.62(8)	0.3864(16)	− 0.003(3)	0.2311(10)	0.58(3)	0.89(4)
O4	4*g*	0.141	− 0.022	0.117	0.62(8)	0.1261(14)	− 0.0414(21)	0.1057(9)	0.58(3)	
O5	4*g*	0.107	0.055	0.430	0.62(8)	0.1285(14)	0.0717(24)	0.4363(9)	0.58(3)	
O6	4*g*	0.106	− 0.005	0.264	0.62(8)	0.1149(18)	0.0265(23)	0.2678(11)	0.58(3)	0.90(4)
O7	4*g*	0.114	0.448	0.014	0.62(8)	0.1214(15)	0.4442(24)	0.0231(9)	0.58(3)	
O8	4*g*	0.125	0.567	0.349	0.62(8)	0.1244(16)	0.5413(25)	0.3472(10)	0.58(3)	
O9	4*g*	0.121	0.502	0.173	0.62(8)	0.1242(15)	0.5280(21)	0.1880(9)	0.58(3)	0.93(4)
O10	4*g*	0.398	0.451	0.478	0.62(8)	0.3868(14)	0.4484(23)	0.4760(9)	0.58(3)	
O11	4*g*	0.388	0.516	0.142	0.62(8)	0.3769(14)	0.5422(22)	0.1498(10)	0.58(3)	
O12	4*g*	0.381	0.488	0.301	0.62(8)	0.3895(15)	0.4775(24)	0.3074(10)	0.58(3)	0.88(4)

coordinates and occupancy factors for sites which had not been found fully occupied within standard uncertainty were also refined during the last cycles (102 parameters). Diffraction data in the range $22^\circ \leq 2\theta \leq 160^\circ$ contained 2211 reflections from $Ca_5Cu_6O_{12}$, 103 from Ca_2CuO_3, 15 from CaO, and 81 from CuO. The background and the diffraction peaks were fitted with a polynomial function and a pseudo-Voigt profile function, respectively. Refinement results are given in Tables 2 and 3 and selected interatomic distances presented in Tables 4 and 5. The observed and calculated diffraction patterns for samples S1 (X-ray) and S2 (neutrons) are shown in Fig. 4.

Both structure refinements resulted in a rather good agreement between observed and calculated patterns as can be seen from Table 2 and Fig. 4. Note in particular the low value of the residual on the observed superstructure reflections only: $R_{\text{Bragg}} = 5.75\%$ (neutron data). The structure model is therefore correct. However, although refined Cu atom coordinates are very similar in both cases, small but significant differences are observed for Ca and O atom positional parameters (Table 3). The discussion on the structure of $Ca_5Cu_6O_{12}$ (see Section 5.1) is based on neutron data analysis only which is certainly more reliable.

4.2. Tl-Containing Samples

Tl-containing samples were first characterized by SEM EDX. The Tl content in the $(Ca_{1-x}Tl_x)_{1-y}CuO_2$ phase was found larger in S4 than in S3 and no gold contamination could be detected in the bulk of either sample. Attempts to refine the structure of $(Ca_{1-x}Tl_x)_{1-y}CuO_2$ in the supercell of the Tl-free phase were unsuccessful because of the significant angular shift of some superstructure reflections. The X-ray diffraction patterns of S3 and S4 are presented in Fig. 5. The four main superstructure lines in the pattern of S3 merge into two lines in the pattern of S4. In addition, when S4 is heated in flowing oxygen up to 950°C (just below the decomposition temperature), causing a small Tl loss, the two lines split into four (S4dta; Fig. 5). It is therefore believed that the substitution of Ca atoms by Tl atoms produces incommensurate modulations and that the modulation vector(s) is (are) strongly dependent on the Tl content. The parameters of the *Fmmm* subcell of $(Ca_{1-x}Tl_x)_{1-y}CuO_2$ in S2, S3, S4, and S4dta are given in Table 6. Note that although $(Ca_{1-x}Tl_x)_{1-y}CuO_2$ in S4 and S4dta have different modulations, the parameters of their subcell are strictly identical.

TABLE 4
Ca–O and Cu–O Distances (Å) in the Structure of $Ca_5Cu_6O_{12}$ from Neutron Data Rietveld Analysis

Cu1–O4	1.969(15)	Cu2–O4	2.012(20)
Cu1–O4	1.969(15)	Cu2–O5	1.995(19)
Cu1–O5	2.027(16)	Cu2–O6	1.818(22)
Cu1–O5	2.027(16)	Cu2–O6	1.810(23)
⟨Cu1–O⟩	1.998(16)	⟨Cu2–O⟩	1.909(21)
Cu3–O7	1.897(20)	Cu4–O8	1.845(17)
Cu3–O7	1.849(19)	Cu4–O8	1.845(17)
Cu3–O8	2.054(21)	Cu4–O9	1.917(16)
Cu3–O9	2.035(18)	Cu4–O9	1.917(16)
⟨Cu3–O⟩	1.959(20)	⟨Cu4–O⟩	1.881(17)
Cu5–O1	2.053(14)	Cu6–O1	1.957(19)
Cu5–O1	2.053(14)	Cu6–O2	1.859(19)
Cu5–O2	2.037(17)	Cu6–O3	1.859(22)
Cu5–O2	2.037(17)	Cu6–O3	1.859(21)
⟨Cu5–O⟩	2.045(16)	⟨Cu6–O⟩	1.884(20)
Cu7–O10	1.813(21)	Cu8–O11	1.880(16)
Cu7–O10	1.885(20)	Cu8–O11	1.880(16)
Cu7–O11	1.980(21)	Cu8–O12	1.744(17)
Cu7–O12	1.979(21)	Cu8–O12	1.744(17)
⟨Cu7–O⟩	1.914(21)	⟨Cu8–O⟩	1.812(17)
Ca1–O1	2.256(23)	Ca2–O2	2.462(25)
Ca1–O2	2.438(23)	Ca2–O4	2.282(24)
Ca1–O5	2.405(24)	Ca2–O5	2.306(24)
Ca1–O7	2.353(24)	Ca2–O7	2.308(24)
Ca1–O8	2.298(23)	Ca2–O10	2.499(24)
Ca1–O10	2.402(24)	Ca2–O11	2.309(24)
⟨Ca1–O⟩	2.359(24)	⟨Ca2–O⟩	2.361(24)
Ca3–O1	2.435(27)	Ca4–O2	2.533(24)
Ca3–O5	2.488(28)	Ca4–O3	2.327(24)
Ca3–O6	2.365(27)	Ca4–O4	2.327(22)
Ca3–O8	2.315(29)	Ca4–O7	2.615(22)
Ca3–O10	2.458(25)	Ca4–O9	2.383(23)
Ca3–O12	2.303(29)	Ca4–O11	2.311(23)
⟨Ca3–O⟩	2.393(27)	⟨Ca4–O⟩	2.415(23)
Ca5–O1	2.384(20)		
Ca5–O3	2.277(24)		
Ca5–O6	2.350(24)		
Ca5–O8	2.595(24)		
Ca5–O9	2.228(21)		
Ca5–O12	2.230(23)		
⟨Ca5–O⟩	2.344(23)		

5. DISCUSSION

Comparison between calculated (Table 1, set 1a) and refined atom coordinates (Table 3) for $Ca_5Cu_6O_{12}$ indicates that the displacements of Cu atoms with respect to their positions derived from the *Fmmm* substructure are extremely small. They do not contribute to the formation of the superstructure. However, the displacements of Ca atoms, mainly along [001], and of O atoms along [010] are larger by far and may be understood in terms of a relaxation toward a more regular octahedral environment for Ca atoms. An even distribution of these atoms in the channels would result in a four-fold coordination for Ca5, the four surrounding O atoms forming a distorted tetrahedron (Fig. 6a). This is of course not suitable. For this reason, Ca5 is moved by roughly 0.30 Å as indicated by the arrow in Fig. 6a and now has six neighboring O atoms. The displacements of the other Ca atoms, although less pronounced, are caused by the same requirement and also by Ca^{2+}–Ca^{2+} repulsion. The acceptable, nearly six-fold coordination for Ca atoms is also achieved by the displacements of the O atoms along [010]. Let us consider for example the case of Ca1 (Fig. 6a). In the absence of O atom displacements, it would have two neighboring O atoms, O5 and O10, at a short distance and four others, O1, O2, O7, and O8, at a longer distance. O atoms are therefore moved in such a way that O1, O2, O7, and O8 come closer to Ca5 whereas O5 and O10 are rejected farther away, resulting in similar Ca1–O distances (Table 4). The same remark holds for other Ca atoms so that the range of Ca–O distances is restrained to 2.23–2.62 Å. Moreover the mean Ca–O distances lie between 2.34 and 2.42 Å which is consistent with the values for the Ca^{2+} (VI) and O^{2+} (IV) ionic radii, 1.00 and 1.38 Å, respectively (22). The displacements of Ca and O atoms with respect to their positions in the starting model result in a distorted octahedral coordination for all Ca atoms. Since the O atoms are mainly displaced along [010], the Cu–O distances are affected to the second order only. They remain within the expected range and vary from 1.74 to 2.05 Å (Table 4). For the same reason, the linear chains of edge-shared CuO_4 squares are twisted. Figure 6b shows

TABLE 5
Ca–Ca Spacings (Å) in the Structure of $Ca_5Cu_6O_{12}$ from Neutron Data Rietveld Analysis

Ca1–Ca4	3.418(22)	Ca2–Ca3	3.261(25)
Ca1–Ca5	3.136(22)	Ca2–Ca5	3.675(22)
Ca1–Ca2	3.482(25)	Ca2–Ca1	3.482(24)
Ca1–Ca2	3.617(25)	Ca2–Ca1	3.617(24)
Ca1–Ca3	3.51(3)	Ca2–Ca4	3.591(24)
Ca1–Ca3	3.62(3)	Ca2–Ca4	3.683(24)
⟨Ca1–Ca⟩	3.464(25)	⟨Ca2–Ca⟩	3.551(24)
Ca3–Ca2	3.261(25)	Ca4–Ca1	3.418(22)
Ca3–Ca4	3.363(24)	Ca4–Ca3	3.363(24)
Ca3–Ca1	3.51(3)	Ca4–Ca2	3.591(24)
Ca3–Ca1	3.62(3)	Ca4–Ca2	3.683(24)
Ca3–Ca5	3.47(3)	Ca4–Ca5	3.671(22)
Ca3–Ca5	3.51(3)	Ca4–Ca5	3.675(22)
⟨Ca3–Ca⟩	3.46(3)	⟨Ca4–Ca⟩	3.567(23)
Ca5–Ca1	3.136(22)		
Ca5–Ca2	3.675(22)		
Ca5–Ca3	3.47(3)		
Ca5–Ca3	3.51(3)		
Ca5–Ca4	3.671(22)		
Ca5–Ca4	3.675(22)		
⟨Ca5–Ca⟩	3.523(25)		

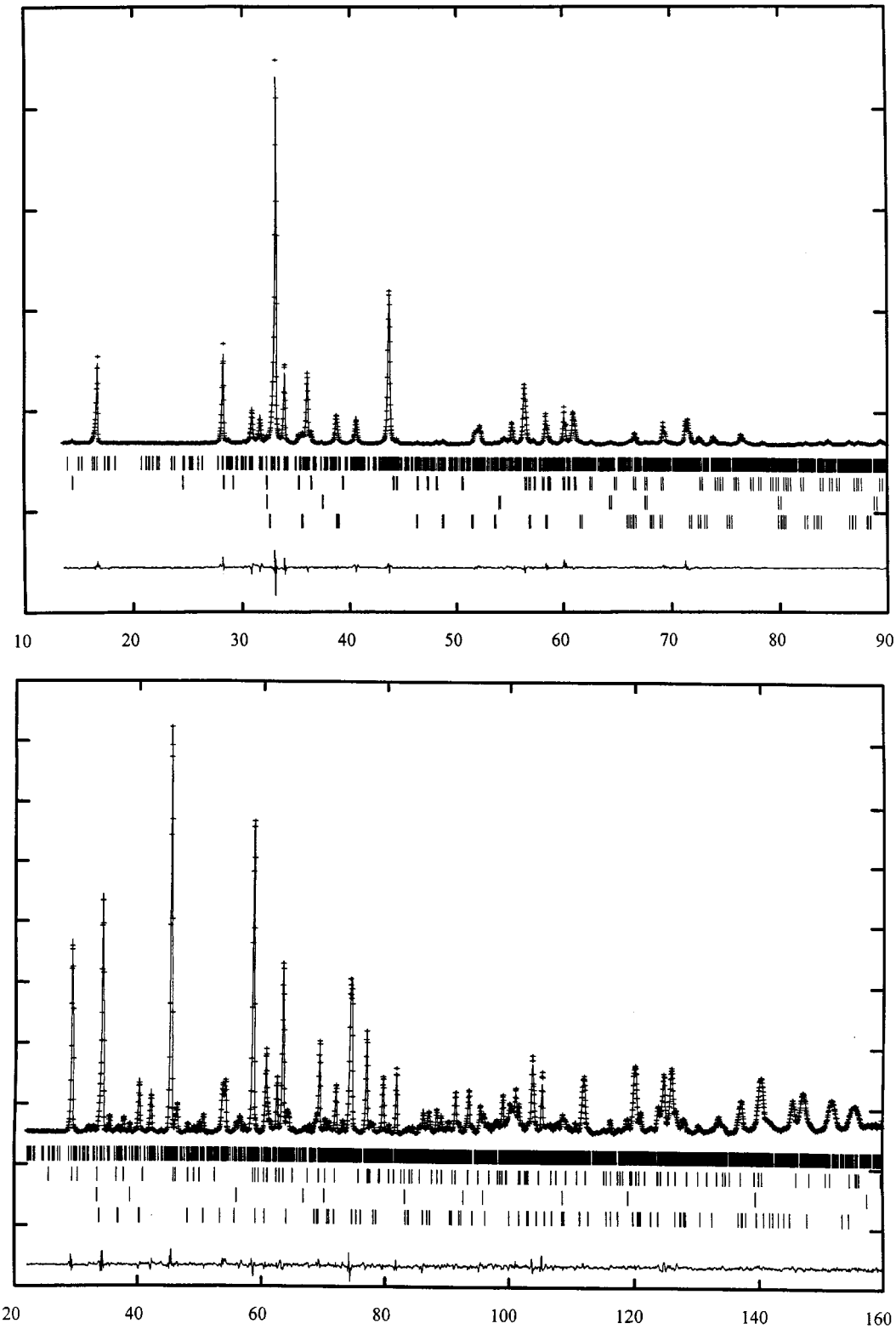

FIG. 4. Observed (+ signs), calculated (solid line), and difference (bottom) diffraction patterns for samples S1 (X-ray, top) and S2 (neutrons, bottom) in 2θ. Vertical bars indicate the peak positions of (1) $Ca_5Cu_6O_{12}$, (2) Ca_2CuO_3, (3) CaO, and (4) CuO.

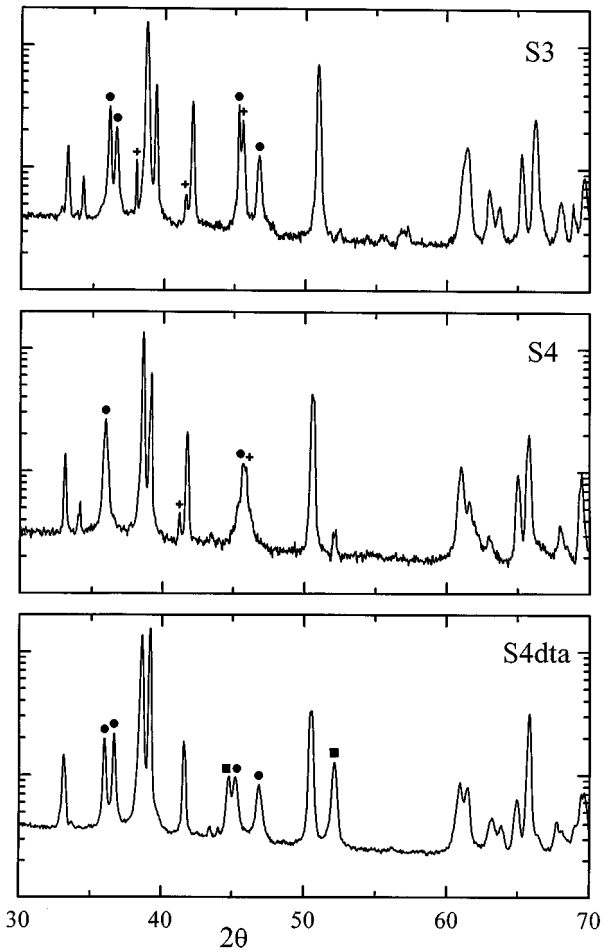

FIG. 5. X-ray diffraction patterns (Co$K\alpha$) of S3, S4, and S4dta. The closed circles denote superstructure reflections from $(Ca_{1-x}Tl_x)_{1-y}CuO_2$, the squares and the crosses the reflections from the Al sample holder and the impurity phases, respectively. 2θ angular range, 30–70°; logarithmic representation.

a projection of the oxygen sublattice along [100]. The amplitude of the quasi sinusoidal displacements of the O atoms is roughly 0.5 Å.

The reason the stoichiometry is $Ca_5Cu_6O_{12}$, or rather $Ca_{4.78}Cu_6O_{11.60}$ taking into account site occupancies, and not $CaCuO_2$ is easily understood. Adding a sixth Ca site in the channels would result in very short Ca–O and Ca–Ca distances. In contrast, the refinement results show that the Ca–O distances are within the expected range and that the Ca–Ca spacings (Table 5) compare well with the Ca–Ca separations found in Ca_2CuO_3 (23) or $CaCu_2O_3$ (24). The Ca–Ca repulsion is therefore minimized. $CaCuO_2$ phases indeed exist but they are prepared at high pressure only and have completely different structures (25, 26). Surprisingly, $Sr_{4.38}Cu_6O_{12}$ (or $Sr_{0.73}CuO_2$), with a structure similar to that of $Ca_5Cu_6O_{12}$, is also prepared at high pressure (27). The particular value of the Ca:Cu ratio in the title compound has another consequence: six O atoms have five neighboring cations while the six others have only four. As can be seen from Table 3, the Ca3, O3, O6, O9, and O12 sites were found partly occupied which yields a refined stoichiometry of $Ca_{4.78}Cu_6O_{11.60}$ (or $Ca_{0.80}CuO_{1.93}$) and an average copper valence of 2.28^+. The partial occupancy of the Ca3 site may be explained by the relatively short distances to the Ca2 and Ca4 sites. Similarly,the mean distances between the O3, O6, O9, and O12 sites and their neighboring cation sites ranges from 2.06 to 2.14 Å while it is larger than 2.22 Å for the other O sites. This may be the cause of the observed deficiency. The oxygen content has been studied by Mathews *et al.* (28) from the weight change under H_2 reduction and emf measurements as a function of oxygen partial pressure. Both methods led to the same result at 1073 K, 11.58(6), in good agreement with our refined value.

Bond valence sums have been computed for Cu and Ca atoms and are reported in Table 7. The resulting values for Cu atoms should be considered with caution since (i) the stoichiometry of the phase implies noninteger values for the average and, most probably, for some individual valences and (ii) the bond strength parameters for Cu^+–O^{2-} and Cu^{3+}–O^{2-} bonds have not been determined as precisely as the parameters for the Cu^{2+}–O^{2-} bond (29). Nevertheless some tendencies clearly appear. In particular, the valences for Cu5 and Cu8 are definitely close to $+1$ and $+3$, respectively. These results could give additional clues for the understanding of the low-temperature magnetic properties of the phase which have been interpreted in terms of the presence of Cu^{3+} ions (14) or Zhang–Rice singlets (30). Note eventually that the average bond sum for Ca is very close to 2.00.

The substitution of Tl for Ca results in an increased thermal stability. Differential thermal analysis and thermogravimetry experiments carried out in flowing oxygen up to 1000°C on sample S4 showed that the decomposition occurs at 970°C (31). It is accompanied by a complete TlO_z release and the resulting powder contains only Ca_2CuO_3 and $CaCu_2O_3$ after rapid cooling which is consistent with the phase equilibrium diagram of the pseudobinary system CaO–CuO (2, 32). An increased thermal stability was also

TABLE 6
Parameters of the Orthorhombic Subcell of $Ca_5Cu_6O_{12}$ and Tl-Containing Phases

	a (Å)	*b* (Å)	*c* (Å)
S2	2.8058(1)	6.3169(2)	10.5758(4)
S3	2.816(1)	6.267(2)	10.618(3)
S4	2.831(3)	6.273(7)	10.67(1)
S4dta	2.832(2)	6.277(6)	10.675(8)

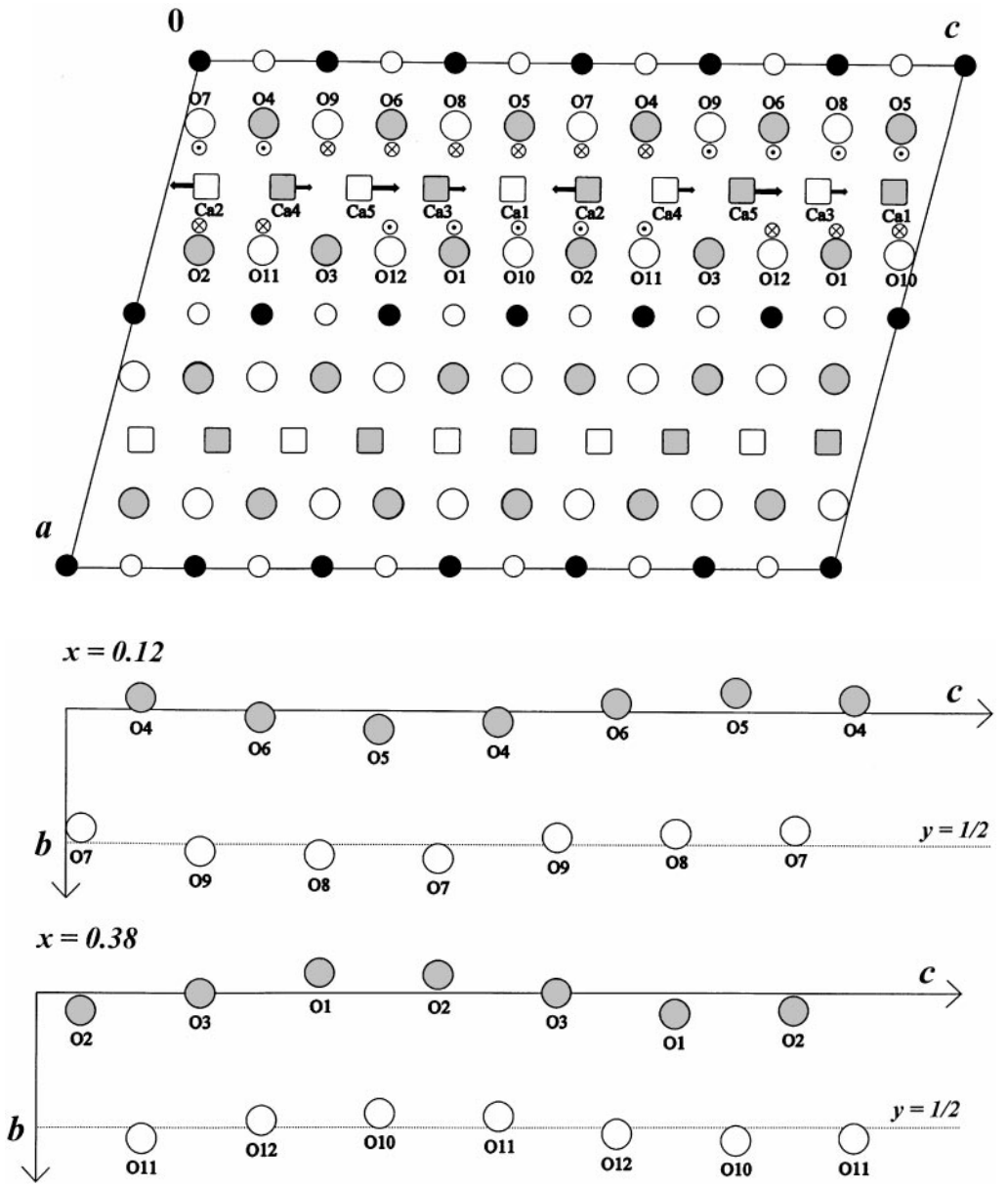

FIG. 6. (a) Schematic drawing of the structure of $Ca_5Cu_6O_{12}$. Arrows indicate the displacements of atoms with respect to their position in the calculated structure (set 1a). The symbols for atoms are the same as in Fig. 2. (b) Projections of the oxygen atom sublattice along [100] showing the quasi sinusoidal displacements of O atoms.

observed for $(Ca_{1-x}M_x)_{1-y}CuO_2$ with M = Y, Nd, and Gd and attributed to a lower oxidation state of copper due to the heterovalent substitution (12). From a structural point of view, the effect of Tl doping appears to be qualitatively similar to that of Nd doping. In the Nd system also, the four main superstructure reflections move significantly when the ratio Ca:Nd is changed and finally merge into two reflections at the solubility limit of composition $Ca_{1.25}Nd_{2.50}Cu_5O_{10}$ (1000°C in air) (12). It is therefore expected that the modulation vectors vary continuously with the Tl content.

6. SUMMARY

The crystal structure of $Ca_{4.78}Cu_6O_{11.60}$ (space group $P2/c$, $a = 10.9456(4)$ Å, $b = 6.3192(2)$ Å, $c = 16.8408(5)$ Å, and $\beta = 104.952(2)^\circ$) has been solved and refined using X-ray and neutron powder diffraction. It is deduced from the previously reported orthorhombic substructure (space group $Fmmm$, $a = 2.807(1)$ Å, $b = 6.351(2)$ Å, and $c = 10.597(3)$ Å) (3) by applying the transformation $\mathbf{a}_m = \mathbf{c}_0 - \mathbf{a}_0$, $\mathbf{b}_m = -\mathbf{b}_0$, and $\mathbf{c}_m = 6\mathbf{a}_0$. The phase stoichiometry

TABLE 7
Bond Valence Sums for Cu and Ca Atoms in the Structure of $Ca_5Cu_6O_{12}$ ($\sum \exp(R_0-R)/B_0$) with $B_0 = 0.37$)

	Σ_1	Σ_2	Σ_3	Σ_S		Σ'_2
R_0 (Å)	1.610	1.679	1.739			1.967
Cu1	1.41(3)	1.70(4)		$\Sigma_{12} = 1.58(5)$	Ca1	2.11(6)
Cu2		2.09(6)		$\Sigma_2 = 2.09(6)$	Ca2	2.12(6)
Cu3		1.91(5)		$\Sigma_2 = 1.91(5)$	Ca3	1.85(6)
Cu4		2.26(5)	2.65(6)	$\Sigma_{23} = 2.43(9)$	Ca4	1.86(6)
Cu5	1.24(3)	1.49(3)		$\Sigma_{12} = 1.32(4)$	Ca5	2.17(6)
Cu6		2.18(6)	2.57(7)	$\Sigma_{23} = 2.30(9)$		
Cu7		2.11(6)	2.48(7)	$\Sigma_{23} = 2.18(9)$		
Cu8		2.64(6)	3.11(7)	$\Sigma_3 = 3.11(7)$		
⟨Cu⟩				$\langle\sum\rangle = 2.12(7)$	⟨Ca⟩	$\langle\sum\rangle = 2.02(6)$

Note. Σ_1, Σ_2, and Σ_3 are defined to be respectively the copper valences assuming Cu^{+}–, Cu^{2+}–, and Cu^{3+}–O^{2-} bond strength parameters. Σ_{12} (Σ_{23}), given by the equation $(\Sigma_{12} - \Sigma_1)/(\Sigma_2 - \Sigma_1) = \Sigma_{12} - 1((\Sigma_{23} - \Sigma_2)/(\Sigma_3 - \Sigma_2) = \Sigma_{23} - 2)$, represent an internally consistent measure of the copper valence when it is between 1 and 2 (2 and 3). These equations were used when the calculated and the assumed integer valences differed by more than 5%. Σ'_2 is the calcium valence.

which gives rise to the six-fold superstructure and the displacements of atoms with repsect to their positions in the subcell are due to the minimization of Ca–Ca repulsion and to a relaxation toward a more regular octahedral coordination for Ca atoms. Tl doping leads to an increased thermal stability and incommensurate structures with modulation vectors depending strongly on the Tl content. Additional work on the structure of $(Ca_{1-x}Tl_x)_{1-y}CuO_2$ and on phase equilibria in the CaO–Tl_2O_3–CuO pseudoternary system is presently under way in our laboratory.

ACKNOWLEDGMENTS

The authors acknowledge fruitful discussions with E. Suard and J. L. Soubeyroux.

REFERENCES

1. M. Lomello-Tafin, Ph. Galez, Th. Hopfinger, J. Allemand, Ch. Bertrand, R. E. Gladyshevkii, M. Couach, and J. L. Jorda, CALPHAD XXVIII, May 2–7, 1999, Grenoble, Collected abstracts 100.
2. R. S. Roth, C. J. Rawn, J. J. Ritter, and B. P. Burton, *J. Am. Ceram. Soc.* **72,** no. 8, 1545 (1989).
3. T. Siegrist, R. S. Roth, C. J. Rawn, and J. J. Ritter, *Chem. Mater.* **2,** 192 (1990).
4. T. G. N. Babu and C. Greaves, *Mater. Res. Bull.* **26,** 499 (1991).
5. C. Dong, H. M. Duan, W. Kiehl, A. Naziripour, J. W. Drexler, and A. H. Hermann, *Physica C* **196,** 291 (1992).
6. N. E. Brese, M. O'Keeffe, R. B. von Dreele, and V. G. Young, *J. Solid State Chem.* **83,** 1 (1989).
7. O. Milat, G. Van Tendeloo, S. Amelinckx, T. G. N. Babu, and C. Greaves, *J. Solid State Chem.* **97,** 405 (1992).
8. O. Milat, G. Van Tendeloo, S. Amelinckx, T. G. N. Babu, and C. Greaves, *Solid State Commun.* **79,** no. 12, 1059 (1991).
9. O. Milat, G. Van Tendeloo, S. Amelinckx, T. G. N. Babu, and C. Greaves, *J. Solid State Chem.* **101,** 92 (1992).
10. S. Kikkawa, N. Kato, N. Taya, M. Tada, and F. Kanamaru, *J. Am. Ceram. Soc.* **78,** no. 5, 1387 (1995).
11. P. K. Davies, E. Caignol, and T. King, *J. Am. Ceram. Soc.* **74,** no. 3, 569 (1991).
12. P. K. Davies, *J. Solid State Chem.* **95,** 365 (1991).
13. Y. Miyazaki, I. Gameson, and P. P. Edwards, *J. Solid State Chem.* **145,** 511 (1999).
14. J. Dolinšek, D. Arcon, P. Cevc, O. Milat, M. Miljak, and I. Aviani, *Phys. Rev. B* **57,** no. 13, 7798 (1998).
15. H. Yamaguchi, K. Oka, and T. Ito, *Physica C* **320,** 167 (1999).
16. M. Matsuda, K. Ohyama, and M. Ohashi, *J. Phys. Soc. Jpn.* **68,** 269 (1999).
17. H. F. Fong, B. Keimer, J. W. Lynn, A. Hayashi, and R. J. Cava, *Phys. Rev. B* **59,** 6873 (1999).
18. A. Hayashi, B. Batlogg, and R. J. Cava, *Phys. Rev. B* **58,** 2678 (1998).
19. E. M. McCarron III, M. A. Subramanian, J. C. Calabrese, and R. L. Harlow, *Mater. Res. Bull.* **23,** 1355 (1988).
20. T. Siegrist, L. F. Schneemeyer, S. A. Sunshine, and J. V. Waszczak, *Mater. Res. Bull.* **23,** 1429 (1988).
21. J. Rodriguez-Carvajal, Fullprof, Version 3.5d, October 98, Laboratoire Leon Brillouin (CEA-CNRS), Saclay, France.
22. R. D. Shannon, *Acta Crystallogr. A* **32,** 751 (1976).
23. Ch. L. Teske and H. K. Müller-Buschbaum, *Z. Anorg. Allg. Chem.* **379,** 234 (1970).
24. Ch. L. Teske and H. K. Müller-Buschbaum, *Z. Anorg. Allg. Chem.* **370,** 134 (1969).
25. J. Karpinski, H. Schwer, I. Mangelschots, K. Conder, A. Morawski, T. Lada, and A. Paszewin, *Physica C* **234,** 10 (1994).
26. N. Kobayashi, Z. Hiroi, and M. Takano, *J. Solid State Chem.* **133,** 274 (1997).
27. J. Karpinski, H. Schwer, G. I. Meijer, K. Conder, E. M. Kopnin, and C. Rossel, *Physica C* **274,** 99 (1997).
28. T. Mathews, J. P. Hajra, and K. T. Jacob, *Chem. Mater.* **5,** no. 11, 1669 (1993).
29. A. S. Wills and I. D. Brown, *VaList*, CEA, France, 1999, program available from authors at willsas@netscape.net.
30. A. Hayashi, B. Batlogg, and R. J. Cava, *Phys. Rev. B* **58,** no. 5, 2678 (1998).
31. M. Lomello-Tafin, K. Jondo, Th. Hopfinger, C. Opagiste, Ch. Bertrand, Ph. Galez, and J. L Jorda, in preparation.
32. D. Risold, B. Hallstedt, and L. J. Gauckler, *J. Am. Ceram. Soc.* **78,** no. 10, 2655 (1995).